SCIENCE CHINA
Chemistry

• ARTICLES •
· SPECIAL TOPIC · Molecular Functional Materials and Applications

June 2016 Vol.59 No.6: 692–698
doi: 10.1007/s11426-015-0538-1

Negative effect on molecular planarity to achieve organic ternary memory: triphenylamine as the spacer

Shugang Xia, Jinghui He, Hua Li, Qingfeng Xu, Najun Li, Dongyun Chen & Jianmei Lu*

College of Chemistry, Chemical Engineering and Materials Science, Collaborative Innovation Center of Suzhou Nano Science and Technology, Soochow University, Suzhou 215123, China

Received December 24, 2015; accepted January 13, 2016; published online May 12, 2016

Adjusting the spacers between the electron-acceptor and the elector-donor is important to design organic ternary memory material but rarely reported. In this paper, two small molecules, ZIPGA and ZIPCAD with benzene ring or triphenylamine as the spacers, were designed and synthesized to fabricate memory devices. The Al/ZIPGA/indium-tin oxide (ITO) device showed ternary characteristics, whereas Al/ZIPCAD/ITO had no obvious memory characteristics. Density functional theory calculation, X-ray diffraction (XRD) and atomic force microscopy (AFM) were employed to interpret the different memory properties. ZIPGA thin film has the closer intermolecular packing and flatter surface morphology than ZIPCAD film, which was favorable to the electron migration. This work demonstrates the importance of spacers and reveals that triphenylamine may be not a good spacer in design of new memory material.

small molecules, different spacers, ternary memory device, molecular stacking

Citation: Xia S, He J, Li H, Xu Q, Li N, Chen D, Lu J. Negative effect on molecular planarity to achieve organic ternary memory: triphenylamine as the spacer. *Sci China Chem*, 2016, 59: 692–698, doi: 10.1007/s11426-015-0538-1

1 Introduction

As the era of information explosion emerges, currently used memory devices have almost reached their limitation due to the difficulty in downscaling to further increase the data-storage density [1–4]. Thus, novel data-storage materials with super-high density have attracted intensive attention of scientists in the last two decades. Recently, small molecules are widely applied as electronic materials due to their tunable structure, low cost, good scalability, facile purification and reproducible performance [5–9]. After years of research, small molecule-based materials were successfully introduced into the fabrication of binary memory devices, which largely increased the data-storage density [10]. Compared to downscaling techniques, multilevel (e.g. ternary) storage can increase the information density dramatically from 2^n to 3^n or higher. After the report about a ternary memory device fabricated with a small molecule, many excellent ternary data-storage devices were successfully designed through tailoring molecular conjugation length, changing the side-chains, introducing different terminal acceptors, or tuning the bridging spacers. On the whole, all these methods will result in the modulation of molecular planarity and molecular stacking in film state, which is an important factor to affect the memory behaviors [11–13]. Among them, adjusting the spacers between the electron-acceptor and the elector-donor is reported to improve monomolecular electronic effect [14,15].

In this paper, we investigated the effects of triphenylamine and benzene as the spacers on the memory performance. Trih-

*Corresponding author (email: lujm@suda.edu.cn)

penylamine has been widely used as an electron donor in organic devices, such as solar cells, optoelectronics, and transistors [16,17], but not employed as a spacer in molecular backbone. TPA as the electron donor in the design of organic memory device has been widely reported. Where there are sufficient electron donors in a molecule, the electron donating properties could be partially omitted. We designed two small molecules, ZIPGA and ZIPCAD (Scheme 1), consisting of a carbazole unit as the electron-donor, while nitro group and benzothiazole serve as two electron-acceptors [18]. The spacer between the nitro and carbazole moieties of ZIPGA is a benzene ring, while for ZIPCAD, the bridge is a triphenylamine (TPA) unit. However, TPA as a spacer, namely a link bridged electron-donating moiety and electron-withdrawing unit will mainly cause changes to geometric property such as planarity, and thus influence the data-storage performance.

The ZIPGA-based memory device exhibited the ternary memory behavior whereas ZIPCAD-based device showed no obvious memory performance. Simulation suggests that the dihedral angles between the spacers and the carbazole moieties showed large difference. Thus, the planarity of these two molecules is different and leads to distinct molecular stacking in film state as confirmed by X-ray diffraction (XRD) and atomic force microscopy (AFM) measurements. This work shows that the spacers in a conjugated molecular backbone plays a crucial role on molecular stacking and thus affects the storage property.

2 Experimental

2.1 Materials

Triphenylamine (98%) and 3-formyl-*N*-ethylcarbazole (98%) were purchased from J&K, China; *N*-bromosuccinimide (98%), carbon tetrachloride (97%), acetic anhydride (98%), copper nitrate trihydrate (97%), bis(pinacolato)diboron (97%), 2-aminothiophenol (97%), potassium acetate (97%), methylbenzene (97%) were purchased from TCI, Japan; 1-bromo-4-nitrobenzene (98%) was purchased from Alfa Aesar, USA; all solvents were purchased from commercial companies without further purification. Compounds **1** to **8** were synthesized according to the methods described in the literature [19–23].

2.2 Molecular synthesis

2.2.1 *N*,*N*-diphenyl-4-bromoaniline (**1**)

Triphenylamine (24 mmol, 5.88 g) and *N*-bromosuccinimide (NBS, 24 mmol, 4.28 g) were dissolved in CCl_4 (50 mL). The solution was refluxed for 4 h in the darkness. The insoluble substance was filtered, and the solvent was then extracted from the solution with dichloromethane (DCM) and washed thoroughly with saturated saline solution. The solution was dried then the remaining from the solvent was recrystallized with ethanol. The obtained white crystalline powder through the suction filter was dried in a vacuum oven (6.8 g, 87%). ^{1}H NMR (400 MHz, $CDCl_3$) δ 7.3–7.13 (m, 6H), 7.06–6.95 (m, 6H), 6.88 (d, J=8.1 Hz, 2H).

2.2.2 4-Bromo-*N*-(4-nitrophenyl)-*N*-phenylaniline (**2**)

Bromotriphenylamine (6.61 mmol, 2 g) and copper nitrate trihydrate (3.08 mmol, 0.75 g) dissolved in acetic anhydride were stirred for 4 h to get the light yellow product (2.02 g, 83%). ^{1}H NMR (400 MHz, $CDCl_3$) δ 8.02–7.94 (m, 2H), 7.43–7.36 (m, 2H), 7.19 (s, 1H), 7.31 (m, 2H). 7.09 (d, J=8.2 Hz, 2H), 6.97 (t, J=8.8 Hz, 2H), 6.92–6.82 (m, 2H).

2.2.3 4-Nitro-*N*-phenyl-*N*-(4-(4,4,5,5-tetramethyl-1,3,2-dioxaborolan-2-yl)phenyl)aniline(**3**)

Compound **2** (5.7 mmol, 2 g) and bis(pinacolato)diboron (8.6 mmol, 2.2 g) were dissolved in toluene (50 mL), then dry potassium acetate (17 mmol, 1.67 g) was added quickly. It was important to keep the reaction dry. The catalyst dppf-$PdCl_2$ (0.4 mmol, 0.29 g) was dropped into a flask in nitrogen after ten minutes. The mixture was heated to 70 °C for 20 h, then mixture was extracted with water and ethyl acetate. Finally the product(1.22 g, 51%) was obtained from the upper organic phase after rotary evaporation. ^{1}H NMR (400 MHz, $CDCl_3$) δ 7.97 (d, J=9.3 Hz, 2H), 7.71 (d, J=8.4 Hz, 2H), 7.31–7.27 (m, 2H), 7.16–7.13 (m, 1H), 7.10–7.06 (m, 4H), 6.91 (d, J=9.3 Hz, 2H), 1.28 (s, 12H).

2.2.4 6-Bromo-9-ethyl-9*H*-carbazole-3-carbaldehyde (**4**)

NBS (3.02 g, 16.97 mmol) dissolved in 20 mL of DMF and 9-ethyl-9*H*-carbazole-3-carbaldehyde (3.79 g, 16.97 mmol) was added dropwise in ice bath. After 12 h, the mixture was poured into water, stirred and filtered. The crude product was purified recrystallization with ethanol to obtain white needle crystals. 4.20 g, 82%. ^{1}H NMR (400 MHz, DMSO) δ 10.05 (s, 1H), 8.54 (s, 1H), 8.26 (s, 1H), 8.04 (d, J=8.5 Hz, 1H), 7.61 (d, J=8.6 Hz, 1H), 7.48 (d, J=8.5 Hz, 1H), 7.34 (d, J=8.6 Hz, 1H), 4.51 (q, J=7.0 Hz, 2H), 1.33 (t, J=7.0 Hz, 3H).

2.2.5 2-(6-Bromo-9-ethyl-9*H*-carbazol-3-yl)benzo[d]thiazole (**5**)

Compound **4** (4 mmol, 1.21 g) and 2-aminobenzenethiol (6 mmol, 0.75 g) were dissolved in DMSO (30 mL). The solution was refluxed for 3 h at 180 °C. The mixture was poured into water (about 15 mL), stirred and filtered. Yield (1.38 g) 85%, light blue, ^{1}H NMR (400 MHz, DMSO) δ 9.01 (s, 1H), 8.69 (s, 1H), 8.26 (d, J=8.1 Hz, 1H), 8.15 (d, J=8.0 Hz, 1H), 8.05 (d, J=7.9 Hz, 1H), 7.81 (d, J=8.8 Hz, 1H), 7.68–7.63 (m, 2H), 7.55–7.52 (m, 1H), 7.46–7.42 (m, 1H), 4.51 (q, J=6.9 Hz, 2H), 1.33 (t, J=6.9 Hz, 3H).

2.2.6 4,4,5,5-Tetramethyl-2-(4-nitrophenyl)-1,3,2-dioxaborolane (**6**)

1-Bromo-4-nitrobenzene (20 mmol, 4.18 g), bis(pinacolato)diboron (B_2pin_2) (30 mmol, 7.7 g), potassium acetate

(60 mmol, 5.8 g) and toluene (100 mL) all were filled in 250 mL three-neck round-bottom flask. Then Pd(dppf)Cl_2 (0.76 mmol, 0.56 g) was added quickly under N_2 protection. The mixture was refluxed at 70 °C for 24 h. The lower story was extracted with dichloromethane before washed with water and brine. After dried with sodium sulfate and solvent was removed, the crude product was purified by column chromatography. Yield (3.74g) 75%, white solid. ^{1}H NMR (400 MHz, DMSO) δ 8.19 (d, J=8.5 Hz, 2H), 7.97 (d, J=8.5 Hz, 2H), 1.36 (s, 12H).

2.2.7 2-(9-Ethyl-6-(4-nitrophenyl)-9*H*-carbazol-3-yl) benzo[d]thiazole (**7**, ZIPCAD)

A 100 mL round-bottom flask was filled with compound **3** (0.91 mmol, 0.41 g), compound **5** (0.91 mmol, 0.34 g), ethanol (16 mL), toluene (40 mL) and H_2O. (40 mL). Then Pd(dppf)Cl_2 (0.08 mmol, 0.09 g) was added quickly under N_2 protection. The mixture was refluxed at 70 °C for 24 h. The lower story was extracted with dichloromethane before washed with water and brine. After dried with sodium sulfate and solvent was removed, the crude product was purified by column chromatography. Yield (0.46 g) 74%, yellow solid ^{1}H NMR (400 MHz, DMSO) δ 9.08 (s, 1H), 8.83 (s, 1H), 8.25 (d, J=9.1 Hz,1H), 8.15–8.11 (m, 3H), 8.05 (d, J=8.0 Hz,1H), 7.95 (d, J=8.4 Hz, 2H), 7.88 (d, J=8.4 Hz, 1H), 7.81 (d, J=8.4 Hz, 1H), 7.77 (d, J=8.5 Hz, 1H), 7.58–7.43 (m, 4H), 7.38–7.32 (m, 5H), 6.92 (d, J=9.2 Hz, 2H), 4.54 (q, J=7.0 Hz, 2H), 1.39 (t, J=7.0 Hz, 3H).

2.2.8 2-(9-Ethyl-6-(4-((4-nitrophenyl)(phenyl)methyl)phenyl)-9*H*-carbazol-3-yl)benzo[d]thiazole (**8**, ZIPGA)

A 100 mL round-bottom flask was filled with compound **6** (0.75 mmol, 0.08 g), compound **5** (0.75 mmol, 0.37 g), H_2O (30 mL), toluene (25 mL) and ethanol (12 mL). Then Pd(dppf)Cl_2 (0.06 mmol, 0.07 g) was added quickly under N_2 protection. The mixture was refluxed at 70 °C for 20 h. The lower story was extracted with dichloromethane before washed with brine. The crude product was purified by column chromatography after dried with sodium sulfate and solvent was removed. Yield (0.25 g) 80%, light yellow solid. ^{1}H NMR (400 MHz, $CDCl_3$) δ 8.94 (s, 1H), 8.49 (s, 1H), 8.35 (d, J=8.5 Hz, 2H), 8.25 (d, J=8.3 Hz, 1H), 8.10 (d, J=8.0 Hz, 1H), 7.94–7.89 (m, 3H), 7.80 (d, J=8.3 Hz, 1H), 7.56–7.49 (m, 3H), 7.41–7.37 (m, 1H), 4.45 (q, J=6.9 Hz, 2H), 1.52 (t, J=7.0 Hz, 3H).

2.3 Measurements

^{1}H NMR spectra were recorded using an Inova 400 MHz FT-NMR spectrometer. UV-Vis absorption spectra were obtained through a Shimadzu UV-3600 spectrophotometer (Japan) at room temperature. Scanning electron microscope (SEM) images were captured on a Hitachi S-4700 scanning electron microscope (Japan). Cyclic voltammetry (CV) measurements were performed in 0.1 M acetonitrile solution of tetrabutylammonium perchlorate (TBAP) on a Corr-Test CS Electrochemical Workstation analyzer equipped with a platinum gauze auxiliary electrode and an Ag/AgCl reference electrode. The surface morphology of films was probed with a MFD-3D-SA Asylum Research's atomic force microscope (AFM). X-ray diffraction (XRD) patterns were taken on an X'Pert-Pro MPD X-ray diffractometer. Thermal properties were estimated from a PE TGA-7 thermogravimetric analysis system (TGA, Perkin Elmer, USA) under a nitrogen atmosphere at a heating rate of 10 °C min^{-1}, respectively.

2.4 Fabrication of the memory device

The indium-tin oxide (ITO) glass was washed sequentially with distilled water, acetone and ethanol under ultrasonic for 25 min, respectively. Then our synthesized molecules were dissolved in cyclohexanone (10 mg mL^{-1}) and uniformly deposited on the surface of desiccative ITO through spin-coating technique at a rotational speed of 1800 r min^{-1} for 30 s. The thickness of the organic film was estimated to be about 110 nm, which was measured by the investigation of cross section of our samples by scanning electronic microscopic (Figure S1, Supporting Information online). Finally, Al was thermally evaporated onto the film surface with a thickness of around 90 nm and area of 0.0314 mm^2 through a shadow mask to form top electrodes.

3 Results and discussion

3.1 Synthetic routes

Scheme 1 shows the synthetic routes of the two molecules and the detailed synthetic procedure is given in the experimental section.

3.2 Thermal stability

TGA was carried out to measure the thermal stability of the two molecules, which is an important factor to affect the potential application in next-generation memory utilizations. ZIPCAD and ZIPGA were disintegrated for 5% weight loss at 321 and 323 °C (Figure S2), respectively. This demonstrates good thermal stability of the materials and the high

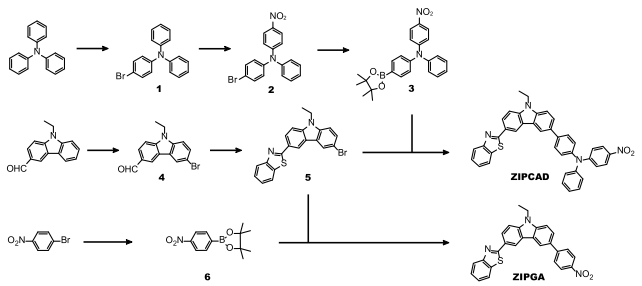

Scheme 1 Synthesis scheme and molecular structures.

thermal decomposition temperature (T_d) values of the small organic molecules implied their potential application in long-term utility.

3.3 Photophysical and electrochemical properties

The UV-Vis spectra of ZIPGA and ZIPCAD were measured in tetrahydrofuran (THF) solution and in film state, respectively. As shown in Figure 1(a), for ZIPGA in the solution state, the maximum absorption peak observed at 314 nm was assigned to the π-π* transition of the carbazole group, while the absorbance peak at 368 nm was attributed to the intermolecular and/or intramolecular charge transfer (CT) process through the molecular backbone [24]. In comparison, the absorption peak in solid state was red-shifted by 50 nm, indicating the ordered stacking of ZIPGA in film state and/or the increased polarizability of the film that was beneficial for the transportation of the charge carriers through the active layers [25–27]. Meanwhile, the UV-Vis spectra were also measured for ZIPCAD in THF and in solid state. The novel absorbance peak located at 353 nm was consistent with the n-π* transition of the TPA moiety. Compared with the absorption spectrum in THF, the absorption spectrum was also red-shifted by about 20 nm in film state, which indicates strong molecular aggregation in film state. Additionally, ZIPGA has a larger red-shift than that of ZIPCAD, which may result from the better planarity of ZIPGA as confirmed in Figure 2.

The electrochemical properties of the two molecules were also measured by CV. For calibration, the absolute redox potential of ferrocene/ferrocenium (Fc/Fc^+) is assumed to be –4.80 eV to vacuum, while the external Fc/Fc^+ redox standard potential is measured to be 0.36 eV vs. Ag/AgCl under the identical condition (Figure S4). As shown in Figure 1(c) amd (d), the first oxidation onset potential of ZIPGA and ZIPCAD was measured to be 0.52 and 0.63 eV, respectively. The HOMO and LUMO energy levels can be calculated by the following equations: HOMO=–[E_{ox}+4.8–$E_{Ferrocence}$]; LUMO=-[E_{red}+4.8–$E_{Ferrocence}$], and the detailed results were shown in Table S1 (Supporting Information online). In addition, according to HOMO and LUMO energy levels, the band-gaps (E_g) of ZIPGA and ZIPCAD were calculated to be about 1.45 and 1.62 eV, respectively. Through calculation, the energy difference between the HOMO level and the work function of ITO was 0.16 eV for ZIPGA, lower than that between the LUMO energy level and the work function of Al (0.79 eV). This indicates that hole injection from ITO into the molecular HOMO energy level is much easier than the electron injection from the Al electrode into the molecular LUMO energy level. Thus, ZIPGA is a p-type material, and the memory behavior is dominated by the hole transportation. Similarly, ZIPCAD is also a p-type material.

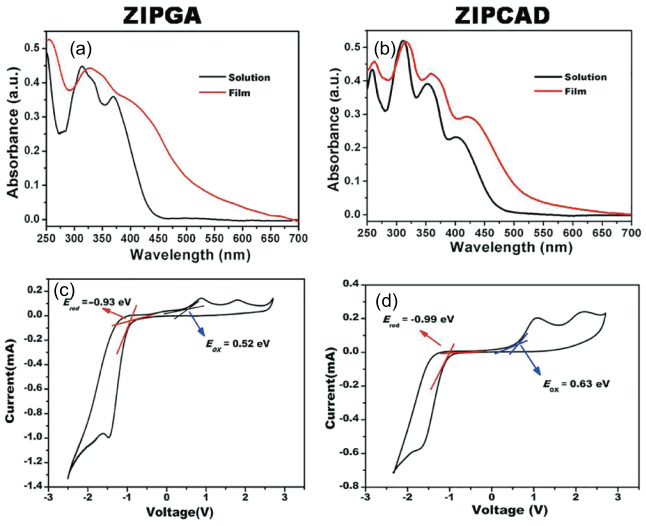

Figure 1 (a, b) UV-Vis absorption spectra of the two molecules in THF solution and on films; (c, d) cyclic voltammograms of the films deposited on ITO glass in CH_3CN (color online).

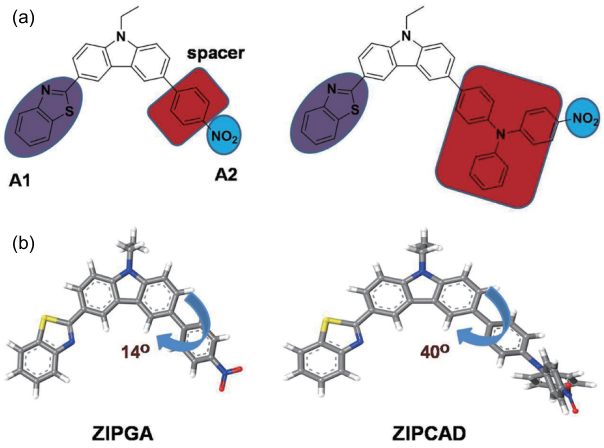

Figure 2 (a) Molecular structures of ZIPGA and ZIPCAD; (b) optimized geometries of ZIPGA and ZIPCAD backbone unites by DFT calculation using the Gaussian 03 with the B3LYP/6-31G (color online).

3.4 Electrical switching effects

Figure 3(a) shows the structural prototype of the fabricated memory device, which consists of an ITO bottom electrode on the glass substrate, an active layer and an Al top electrode. The electrical switching memory characteristics of ZIPGA and ZIPCAD based memory devices were described by the current-voltage (*I-V*) curves under the same condition. As shown in Figure 2(b), ZIPGA based memory device was originally at the low-conductivity (OFF or "0") state. When a voltage sweep from 0 to –5 V was applied on the device, a sudden increase in current was observed from 10^{-8} to 10^{-4} A at the threshold voltage of –3.5 V, implying the transition from low-conductivity (OFF or "0") state to an intermediate-conductance (ON 1 or "1") state. Furthermore, the device could switch to the high-conductivity (ON 2 or "2") state at the threshold voltage of –4.5 V with a current ratio of 10^2 (sweep 1), suggesting the transition from intermediate-conductivity (ON 1 or "1") state to a high-conductivity (ON 2 or

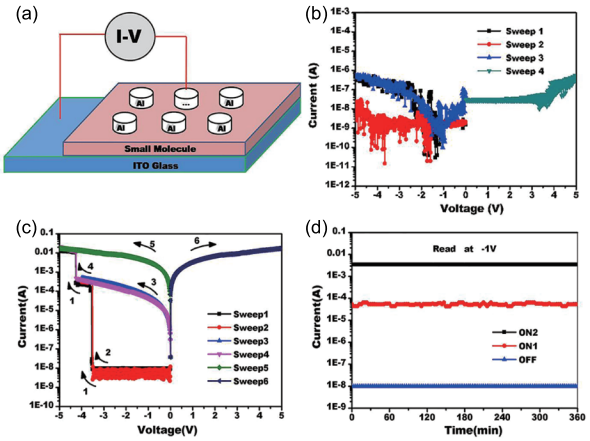

Figure 3 (a) Schematic diagram of sandwich device; (b, c) typical *I-V* characteristics of ZIPGA (b) and ZIPCAD (c) based memory devices; (d) stability test of the ZIPGA based memory device in three states under a constant read voltage of –1 V.

"2") state. Sweep 2 was executed on another cell of the device. When a voltage from 0 to –4 V was applied on the cell, the device can switch from the OFF state to the ON 1 state, and the ON 1 state can be maintained in the following voltage sweep from 0 to –4 V (sweep 3). In the next sweep from 0 to –5 V, the memory device can transfer to the ON 2 state, and the high-conductivity state could be retained under the following sweep from 0 to –5 V (sweep 5). The ON 2 state can even maintain in a reversed voltage sweep from 0 to 5 V (sweep 6) or even the voltage was vanished. These characteristics indicated that the device was a typical ternary WORM (write-once, read-many-times) device. Meanwhile, a reading voltage (e.g. –1.0 V) can be used to read the "0", "1" and "2" signals of the storage device (Figure 2(d)), and no obvious degradation was observed of the current for all the three states. Moreover, the effect of continuous read pulses of –1 V on the OFF, ON 1 and ON 2-states was also investigated (Figure S3). Compared with the device of Al/ZIPGA/ITO, the electric behavior of the ZIPCAD-based device was rather different. As shown in Figure 3(c), ZIPCAD based device showed no obvious memory properties. The device has a decrease of current when the voltage is sweeping from 0 to –1 V (or at 4 V for sweep 4), namely a negative differential resistance (NDR) effect [28,29]. The different memory behaviors for these two molecules based memory devices may be correlated with the molecular stacking in the films, which we will discuss later.

3.5 Morphology of films and molecular packing

To understand the discrepancies of memory behaviors of these two molecules, AFM was used to detect the surface morphology of the spin-coated organic layers. As shown in Figure 4(a), the tapping-mode AFM height image clearly shows that ZIPGA forms a netlike structure in its solid state with uniform size, which illustrated that ZIPGA formed an ordered stacking in film state that is favorable to the mobility of the charge carriers. In addition, the root-means-square (RMS) was measured to be 1.02 nm, indicating that the film was smooth enough that can decrease the energy barrier between the active layer and the electrode. In comparison, the roughness (39 nm) of ZIPCAD film was larger than that of ZIPGA at same temperature and substrate, as shown in Figure 4(b). The large surface roughness indicated that ZIPCAD was self-assembled during the spin-deposition process and would increase the energy barrier between the film and the electrodes [30,31]. Additionally, only amorphous structures were observed for ZIPCAD based film, indicating ZIPCAD has not formed the ordered arrangement. This might be due to the large dihedral angle that causes the relatively weak intramolecular interactions.

X-ray diffraction (XRD) confirms the different molecular crystallinity of these two molecules as observed by AFM. As shown in Figure 5, the X-ray pattern of ZIPGA film is distinct from that of the ZIPCAD film. For ZIPGA based film, two conspicuous peaks were observed at 8.37° and 13.37° with the d-space of 10.56 and 6.64 Å, respectively, indicating that

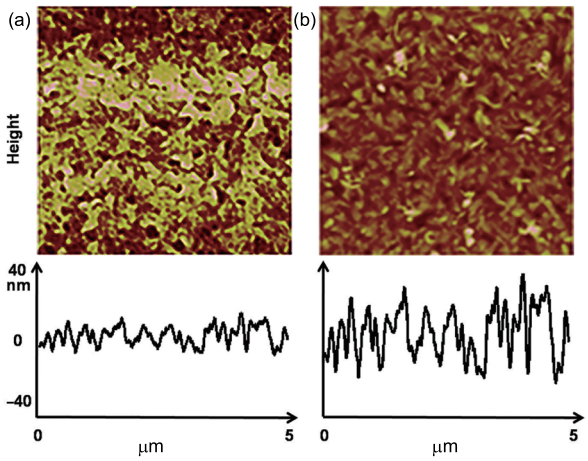

Figure 4 The tapping-mode AFM height images of (a) ZIPGA and (b) ZIPCAD films spin-coated onto ITO glass (color online).

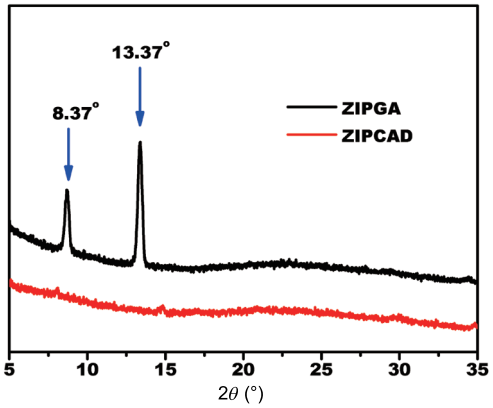

Figure 5 The XRD patterns of ZIPGA and ZIPCAD (color online).

ZIPCAD crystallized well in the film state [32]. The ordered stacking of ZIPCAD in film is beneficial for the migration of the charge carriers through the films and thus facilitates the excellent memory behaviors.

In contrast, the XRD measurement showed no obvious diffraction peaks for ZIPGA based films, implying that ZIPGA was amorphous in film state [33,34]. The amorphous stacking limited the movement of the charge carriers in the films, which is not conductive to the memory performance. Thus, ZIPCAD based memory device showed no memory behaviors. In addition, it was reported that the NDR effect also correlates with the low conductivity of materials, confirming our proposed relationship between crystallinity and memory behaviors [35,36].

3.6 Proposed memory mechanisms

To account for the electrical switching characteristic of the memory devices, theoretical calculations have been performed using the density functional theory (DFT) method with B3LYP/6-31G set. For organic materials with memory switching behavior, charge-trapping mechanism is well proposed [37,38]. DFT molecular simulation results (Figure 6) showed that an open channel is formed from the molecular surface throughout the conjugated backbone with continuous positive molecular electrostatic potential (ESP, in blue), through which charge carriers can migrate freely. The shaded regions of ESP (in yellow) caused by the electron-deficient groups, such as benzothiazole and nitrobenzene segments, can regard as "traps" with different electric charge depths to block the motion of charge carriers. Figure 6(a) shows an integrated process of the charge transport in molecule. In a low voltage bias, the device is in a low-conductivity state due to the big "trap" that hinders the electron migration

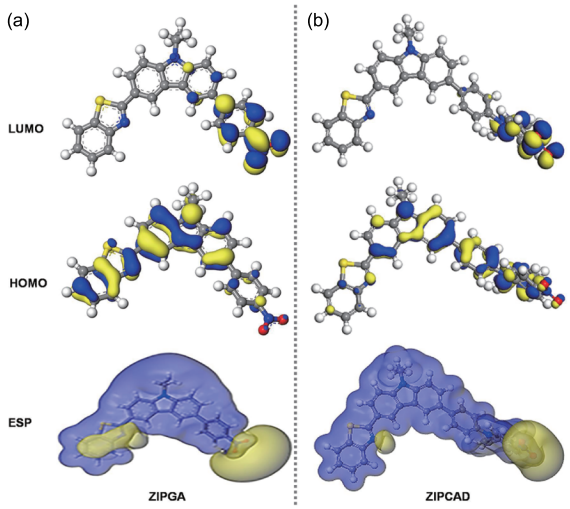

Figure 6 The electrostatic potential (ESP) and frontier molecule orbital (LUMO and HOMO) obtained from DFT calculations on the molecules of ZIPGA and ZIPCAD (color online).

(HOMO). When the external voltage rises to –3.5 V, the trap from benzothiazole acceptor will be filled, leading to the electrical switching from OFF to ON1 state [39]. With the increase of the applied voltage, the traps originated from the nitrobenzene acceptor will be suffused sequentially, leading to the current transition from the ON1 to the ON2 state which implies the second "write" process (LUMO). Upon reaching to the nitro group based deep traps, electrons become more localized. Additionally, the trapped carriers would be stabilized by intermolecular charge transfer. The trapped charge carriers are not released easily even the power was shut down or was reversed, leading to a high-conductivity state that can be sustained permanently [40]. Therefore, the ZIPGA based memory device shows the typical non-volatile WORM behavior.

According to the optimized molecular geometries (Figure 2), it can be obviously observed that the dihedral angle between benzene ring and carbazole plane was 14° for ZIPGA, which was smaller than that of ZIPCAD (40°) between triphenylamine group and carbazole plane. Apparently, the smaller dihedral angle in ZIPGA resulted in a more coplanar configuration than ZIPCAD, which was beneficial to charge transfer [41,42]. Moreover, the non-planar spatial conformation of triphenylamine was not convenient for electron-delocalization or coupling of the frontier orbitals between the donor and acceptors, which impeded the "traps" to be filled. As a result, ZIPCAD based memory devices showed no storage performance, whereas ZIPGA based device showed obvious ternary characteristics. Charge transport mechanism at different conductive states has been also studied by curve fitting (Figure S5). For the *I-V* curve of the ZIPGA-based device, the conduction mechanism at the OFF state, ON1 state and ON2 state can be controlled by thermionic emission, space-charge-limited current and Poole-Frenkel emission. So the conduction mechanism of the ZIPGA device is dominated by charge transport through the electrically charged defect-filled bulk material.

4 Conclusions

In summary, we successfully synthesized two small organic molecules (ZIPGA and ZIPCAD) and tested their electro-resistive memory behaviors. ZIPGA based device showed obvious ternary characteristics including low-conductivity (OFF) state, intermediate-conductance (ON 1) state and high-conductivity (ON 2) state due to the small dihedral angle and the more planar structure. Meanwhile the microstructure of ZIPGA based film is more ordered than that of ZIPCAD based film, which was confirmed by the measurements of UV, AFM and XRD. However, the ZIPCAD based device had no obvious memory property because the big dihedral and disorder packing. Thus triphenylamine may be not a proper spacer to link electron donor/acceptor groups due to

its large torsion in the conjugated chain. Our results illustrate the importance of spacer in the design of memory device.

Acknowledgments This work was supported by the National Natural Science Foundation of China (21176164, 21336005), the Chinese-Singapore Joint Project (2012DFG41900), and the Priority Academic Program Development of Jiangsu Higher Education Institutions (PAPD).

Conflict of interest The authors declare that they have no conflict of interest.

Supporting information The supporting information is available online at http://chem.scichina.com and http://link.springer.com/journal/11426. The supporting materials are published as submitted, without typesetting or editing. The responsibility for scientific accuracy and content remains entirely with the authors.

1 Hagen R, Bieringer T. *Adv Mater*, 2001, 13: 1807–1810
2 Liu CL, Chen WC. *Polym Chem*, 2011, 2: 2169–2174
3 Scott JC, Bozano LD. *Adv Mater*, 2007, 19: 1452–1463
4 Xiao J, Yin Z, Wu Y, Guo J, Cheng Y. *Small*, 2011, 7: 1242–1246
5 Yang Y, Ouyang J, Ma L, Tseng RJH, Chu CW. *Adv Funct Mater*, 2006, 16: 1001–1014
6 Kapetanakis E, Douvas AM, Velessiotis D, Makarona E, Argitis P. *Adv Mater*, 2008, 20: 4568–4574
7 Li H, Xu QF, Li NJ, Ge JF, Lu JM, Gu HW. *J Am Chem Soc*, 2010, 132: 5542–5543
8 Ye C, Peng Q, Li M, Luo J, Tang Z. *J Am Chem Soc*, 2012, 134: 20053–20059
9 Jiang G, Song Y, Guo X, Zhang D, Zhu D. *Adv Mater*, 2008, 20: 2888–2898
10 Rozenberg MJ, Inoue IH, Sanchez MJ. *Phys Rev Lett*, 2004, 92: 178302
11 Guo X, Zhou N, Lou SJ, Hennek JW, Ponce Ortiz R. *J Am Chem Soc*, 2012, 134: 18427–18439
12 Miao S, Li H, Xu Q, Li Y, Ji S. *Adv Mater*, 2012, 24: 6210–6215
13 Miller NC, Sweetnam S, Hoke ET, Gysel R, Miller CE. *Nano Lett*, 2012, 12: 1566–1570
14 Li Y, Li H, Chen H, Wan Y, Li N. *Adv Funct Mater*, 2015, 25: 4246–4254
15 Bao Q, Zhang Q, Li Y, Li H, He J. *Org Electron*, 2016, 28: 155–162
16 Shirota Y. *J Mater Chem*, 2005, 15: 75–93
17 Cravino A , Roquet S , Ale O, Leriche P , Frere P , Roncali J. *Chem Mater*, 2006, 18: 2584–2590
18 Su Z, Liu H, Li H, Lu J, Wang L. *J Mater Chem C*, 2014, 2: 5673
19 Ishiyama T , Murata M , Miyaura N. *J Org Chem*, 1995, 60: 7508–7510
20 Shi HP, Dai JX, Xu L, Shi LW, Fang L. *Org Biomol Chem*, 2012, 10: 3852–3858
21 Yang X, Zhao Y, Zhang X, Li R, Dang J. *J Mater Chem*, 2012, 22: 7136–7148
22 Bala M, Verma PK, Sharma U, Kumar N, Singh B. *Green Chem*, 2013, 15: 1687–1693
23 Banerjee S, Payra S, Saha A, Sereda G. *Tetrahedron Lett*, 2014, 55: 5515–5520
24 Lee WY, Kurosawa T, Lin ST, Higashihara T, Ueda M. *Chem Mater*, 2011, 23: 4487–4497
25 Bromley ST, Mas-Torrent M, Hadley P, Rovira C. *J Am Chem Soc*, 2004, 126: 6544–6545
26 Troisi A, Orlandi G. *J Am Chem Soc*, 2006, 110: 4065–4070
27 Coropceanu A, Cornil J, da Silva Filho DA, Olivier Y, Silbey R, Brédas JL. *Chem Rev*, 2007, 107: 926–952
28 Tu CH, Kwong DL, Lai YS. *Appl Phys Lett*, 2006, 89: 252107
29 Chen J, Xu L, Lin J, Geng Y, Wang L. *Appl Phys Lett*, 2006, 89: 083514
30 Moskovits M. *J Chem Phys*, 1978, 69: 4159–4161
31 Nayfeh A, Chui CO, Saraswat KC, Yonehara T. *Appl Phys Lett*, 2004, 85: 2815–2817
32 Loser S, Bruns CJ, Miyauchi H, Ortiz RP , Facchetti A. *J Am Chem Soc*, 2011, 133: 8142–8145
33 Mukerjee S, Srinivasan S, Soriaga MP, McBreen J. *Phys Chem*, 1995, 99: 4577–4589
34 Thamaphat K, Limsuwan P, Ngotawornchai B. *Nat Sci*, 2008, 42: 357–361
35 You YT, Wang ML, Xuxie HN, Wu B, Sun ZY. *Appl Phys Lett*, 2010, 97: 233301
36 Banerjee I, Harris P, Salimian A, Ray AK. *IET Circ Device Syst*, 2015, 9: 428–433
37 Jeon S, Han JH, Lee J, Choi CJ, Choi S, Hwang H, Kim C. *IEEE Electron Device Lett*, 2005, 52: 2654–2659
38 Li H, Li NJ, Sun R, Gu HW, Ge JF. *J Phys Chem C*, 2011, 115: 8288–8294
39 Hu B, Zhu X, Chen X, Pan L, Peng S. *J Am Chem Soc*, 2012, 134: 17408–17411
40 Zhuang XD, Chen Y, Liu G, Zhang B, Neoh KG. *Adv Funct Mater*, 2010, 20: 2916–2922
41 Grabowski ZR, Rotstyna K, Rettig W. *Chem Rev*, 2003, 103: 3899–4031
42 Dreuw JLW, Head-Gordon M. *J Chem Phys*, 2010, 119: 2943–2946